# CALCULATION OF F/A-18 FATIGUE LOADS AND WING DEFORMATION USING COMPUTATION FLUID DYNAMICS

M. Guillaume*, J. Vos**, A. Gehri*, B. Bucher*, S. Merazzi***, Th. Ludwig***, G. Mandanis****
*RUAG Aerospace, **CFS Engineering, ***SMR SA, ****M@M GmbH

**Keywords**: *Computational Fluid Dynamics, Loads, Fluid Structure Coupling*

## 1. Abbreviations

| | |
|---|---|
| ALE | Arbitrary Lagrange Eulerian |
| AOA | angle of attack |
| ASIP | Aircraft-Structural-Integrity-Program |
| CAD | Computer Aided Design |
| $C_D$ | Drag coefficient for whole aircraft |
| CFD | Computational Fluid Dynamic |
| $C_L$ | Lift coefficient for whole aircraft |
| $C_M$ | Pitching moment for whole aircraft |
| CP | centre of pressure |
| CTR | center |
| FEM | Finite Element Model |
| FUSE | fuselage |
| $F_Z$ | Force in global z direction |
| FWD | forward |
| HT | Horizontal Tail (Höhenleitwerk) |
| HZT | horizontal |
| IGES | 3D CAD format |
| ILEF | Inboard Leading Edge Flap |
| LEX | Leading Edge Extension |
| NSMB | Navier Stokes Multi Block |
| Nz | load factor |
| MPI | Message Passing Interface |
| OEM | Original Equipment Manufacturer |
| OLEF | Outboard Leading Edge Flap |
| q | dynamic pressure |
| RH | right hand |
| SPMD | Single Program Multiple Data |
| TEF | Trailing Edge Flap |
| TOT | total |
| VT | vertical tail |
| W/O | without |

## 2. Introduction

Aerodynamic loads on the F/A-18 aircraft were an important subject during the execution of the Swiss F/A-18 full scale fatigue tests performed at RUAG Aerospace, because only few relevant fatigue load cases for the entire airplane were obtained from The Boeing Company in St. Louis, the F/A-18 Original Equipment Manufacturer (OEM).

These load cases were used originally within the ASIP studies in the 1990s, before the construction of the RUAG full scale fatigue test facility. In the ASIP studies the structural integrity of the entire airframe based on the Swiss flight spectrum was analyzed and a service life of 5000 Swiss flight hours had to be demonstrated. However to reach this goal some structural modifications had to be made to the aircraft, as for instance the change of material from aluminium alloy to titanium for the three carry through bulkhead in the centre fuselage. Furthermore fatigue life improvement technologies (beef-up, cold working, interference fit fasteners) were applied on the wing and the centre fuselage.

The ASIP balanced fatigue load cases correspond to the inertia and aerodynamic forces distributed over the whole aircraft for steady state manoeuvres. To determine these forces mainly the F4 US Navy flight loads data base, containing component loads measured during flight tests, was used. The fitting of the data in order to create a realistic balanced load case was done by adjusting the forces distribution on the different components using

some healthy engineering judgement. This method was not documented in all details and seems not to be always fully rational. This situation pushed RUAG Aerospace to search for methods to generate independently aerodynamic loads for the F/A-18 and as a result a large investment was made in the development and implementation of Computational Fluid Dynamics (CFD). This effort provided RUAG Aerospace with the ability to predict component loads to be applied on the structure for fatigue calculations. In addition, a tool was obtained which permitted to better understand the complicated flow field over the entire F/A-18 full flight envelope and to check some load cases delivered by the OEM.
Section 3 of this paper discusses the development and activities in Computation Fluid Dynamics, while section 4 discusses the results of various studies on the F/A-18 aircraft. Conclusions and a future outlook are presented in Section 5.

## 3. Computational Fluid Dynamic Development

### 3.1 The CFD Solver

The calculations of the F/A-18 flow field were made using the NSMB Structured Multi Block Navier Stokes Solver. NSMB was developed from 1992 until 2003 in a consortium composed of four universities, namely EPFL (Lausanne), SERAM (Paris), IMFT (Toulouse) and KTH (Stockholm) and four industrial companies namely Airbus France, EADS (Les Mureaux), CFS Engineering (Lausanne) and SAAB Aerospace (Linköping). Since 2004 NSMB is developed in a new consortium lead by CFS Engineering and composed of RUAG Aerospace (Emmen), EPFL (Lausanne), EHTZ (Zürich), IMFT (Toulouse), IMFS (Strassbourg) and the Technical University of München.

NSMB employs the cell-centered Finite Volume method using multi block structured grids to discretize the Navier Stokes equations. Various space discretization schemes are available to approximate the inviscid fluxes, among them the 2$^{nd}$ and 4$^{th}$ order centered scheme with artificial dissipation, and 2$^{nd}$, 3$^{rd}$ and 5$^{th}$ order upwind schemes. The viscous fluxes are approximated using a 2$^{nd}$ order approximation.
The space discretization leads to a system of ordinary differential equations, which can be integrated in time using either the explicit Runge Kutta scheme or the semi-implicit LU-SGS scheme. To accelerate the convergence to steady state the following methods are available:

- local time stepping
- implicit residual smoothing (only with the Runge Kutta scheme)
- full multi grid (grid sequencing)
- multi grid
- pre-conditioning for low Mach number
- artificial compressibility for incompressible flows

For unsteady flow calculations the 3$^{rd}$ order Runge Kutta scheme and the Dual Time Stepping method are available.

Different turbulence models have been thoroughly tested and validated for NSMB:

- Baldwin-Lomax algebraic model
- Spalart-Allmaras 1 equation model
- Chien k-ε 2 equations model
- Wilcox k-ω 2 equations model
- Menter Baseline and Shear stress k-ω 2 equations model

The ALE approach is available to simulate the flow on moving grids. Recently a re-meshing algorithm was implemented in NSMB to permit the simulation of the flows on deforming grids, as found for example in Fluid Structure Interaction problems.

NSMB has no limit on the number of blocks used in a calculation. Block interfaces do not need to be continuous since a sliding mesh block interface treatment is available.

The NSMB code was originally written in Fortran 77 and the code is at present a mix of

Fortran 77 and Fortran 90. NSMB was parallelized using the master-slave paradigm in 1995, which was changed to the SPMD paradigm using MPI in 1998. NSMB is saved under cvs for revision control, and automatic testing scripts are used for testing each new release.

### 3.2 The F/A-18 Mesh

The most time consuming process in a CFD simulation is the generation of the grid. This involves different steps. First (if required) the CAD surface needs to be cleaned up, then a multi block topology needs to be set-up, and finally the mesh is generated. For the F/A-18 fighter, these tasks were executed by ICEMCFD in collaboration with Centre of Aerodynamics at RUAG Aerospace in 2001. This permitted RUAG Aerospace to acquire the know-how on mesh generation of complex geometries, and the handling of sub-topologies which for the F/A-18 were used to add or remove the AMRAAM and external fuel tanks.

The surface of the F/A-18 was available in IGES format and had to be cleaned up. Gaps between different surfaces had to be suppressed in order to obtain at the end a unique smooth surface.

The multi block topology was generated using ICEMCFD HEXA (see figure 1). At the start of the project it was known that different configurations with different stores and different control surface deflection were to be treated. Scripts were used for control surface deflections while the sub-topology strategy was used to add or remove external stores. As example, a sub-topology was created for the external fuel tank under the wing (see figure 2). To remove this fuel tank, it was sufficient to replace it by a sub-topology which fills the space taken in by the fuel tank. Once the control surface deflections were defined and the stores were selected it required 1 to 3 days of work to obtain an acceptable grid.

In 2005 it was decided to prepare a new grid which includes more details of the aircraft, as for example the LEX fence, SIWA fins and various antennas. Based on the results of the CFD calculations carried out from 2001 to 2004 it was decided to refine the mesh in different regions. The topology and grid generation were carried out by Mindware in Detroit, USA, in collaboration with RUAG Aerospace. In the new mesh the ICEMCFD replay file functionality was used for control surface deflections and for removing fuel tanks, AMRAAM and LEX fence. With the new grid a change in control surface deflection requires only a minimum amount of tuning to obtain an acceptable grid.

A typical example of a FA-18 configuration is the load case C1S825 (see also Section 4.2) which has the following control surface positions:

- leading edge flap 17.4°
- trailing edge flap 13.4°
- rudder 0° (symmetrical manoeuvre)
- horizontal tail -2.2°

and the mesh characteristics are summarized in Table 1.

| | original mesh | new mesh |
|---|---|---|
| number of blocks | 939 | 2802 |
| number of cells | 7.6 millions | 13.9 millions |
| number of surface cells | 243’000 | 376’000 |

Table 1: mesh characteristics

It can be observed that the number of surface cells is increased with more than 50% for the new mesh. This is at one hand due to the modelling of more details of the F/A-18 (antennas, LEX fence, ..), at the other hand the surface mesh of the new mesh is much finer than on the old mesh. The volume mesh of the new mesh is almost doubled compared to the old mesh.

### 3.3 Aerodynamic Loads Extraction

To permit the calculation of the aerodynamic loads on different aircraft components it was decided to divide the aircraft in different components such that each component has a unique boundary condition type in NSMB. A post processing program was developed that computes the aerodynamic loads on each aircraft component, and translates it into American units. This post processing program also produces the data for the so-called Manhattan plots (see Section 4.4) on the wing and on the vertical tail.

### 3.4 Load Transfer Tool

At high angles of attack (which are typical for high g manoeuvres), the wing has to maintain a very high lift to carry the whole loads on the aircraft. As a result the wing deforms, which can be observed with the eye during the take off from the carrier or during the cycling of the full scale fatigue test. At the wing tip deformations of 0.3 m are quite frequent during a standard manoeuvre mission. One can expect that this change in wing shape will have an influence on the flow field over the wing, and thus on the aerodynamic loads. To investigate this effect a tool was developed to transfer the aerodynamic loads computed using CFD to the NASTRAN finite element model (FEM), and to transfer the computed displacements back to the CFD surface grid. Since the CFD surface grid and the mesh of the structural model are totally different (see figure 8) an interpolation procedure based on volume spline interpolation was implemented such that the computed aerodynamic forces are transferred to the set of structural nodes. NASTRAN then uses these forces to evaluate the corresponding deformation, which is then interpolated to the CFD mesh using again the volume spline interpolation. The re-meshing algorithm implemented in NSMB then generates a new CFD mesh. This method has proved its reliability not only for the smooth deflection of the overall wing but also for the deflection of the control surfaces, which are more sensitive.

## 4. Results of Steady State Calculations

In all calculations discussed here it is assumed that the aircraft is perfectly symmetrical and only symmetrical load conditions were considered until now. Consequently only one half of the aircraft was used in the calculations.

### 4.1 Comparison of CFD Component Loads with Flight Test Data

The component loads of the F4 US Navy flight data base are very reliable measurements and were used to validate the CFD calculation. 15 load cases were simulated with the original mesh, taking into account the real flap positions and for the following conditions:

| load case | M | alt. ft | q psf | AOA ° |
|---|---|---|---|---|
| 241_25_0.1 | 0.834 | 21500 | 444 | 4.2 |
| 241_25_1.1 | 0.842 | 21520 | 452 | 5.2 |
| 241_25_2.0 | 0.847 | 21530 | 458 | 6.6 |
| 241_25_2.9 | 0.849 | 21500 | 461 | 9.1 |
| 241_25_3.8 | 0.840 | 21450 | 452 | 12.3 |
| 241_25_4.4 | 0.826 | 21360 | 438 | 15.1 |
| 241_25_4.7 | 0.819 | 21330 | 431 | 15.5 |
| 241_25_5.3 | 0.800 | 21260 | 413 | 17.7 |
| 241_25_6.0 | 0.770 | 21160 | 384 | 22.0 |
| 241_25_6.5 | 0.740 | 21060 | 356 | 26.3 |
| 241_22_0.0 | 0.787 | 15180 | 515 | 1.9 |
| 241_22_0.6 | 0.788 | 15240 | 515 | 0.0 |
| 241_22_1.3 | 0.791 | 15310 | 516 | -1.7 |
| 241_22_2.0 | 0.792 | 15350 | 517 | -3.3 |
| 241_25_3.2 | 0.793 | 15310 | 519 | -4.6 |

Table 2: F4 flight test load cases

The hinge moment of the control surface is measured with precision during the flight. Using the force on the flap determined with CFD, the pressure point and the hinge line location, the corresponding hinge moment can be calculated for all these load cases. Of course the inertia effects due to the flap mass and the load factor are also taken into account by this calculation. In figures 3 and 4 the cross plots for two different flaps showing the hinge moment of the CFD calculation versus the measured hinge moment are represented. Each load case appears with two points since both the left and the right hand side have been measured in flight. For most load cases the hinge moment lies relatively close to the diagonal, they are relatively well correlated with the flight test data. The differences between left and right hand (points with the same abscissa and slightly different ordinate) for all these symmetrical load cases shows that the flight is not completely symmetrical. For example, a small yaw angle during flight will have an impact on the loads.

### 4.2 Comparison of CFD Component Load Results with ASIP

CFD calculations were made for the following 12 ASIP fatigue load cases:

| Load case | Mach | altitude [ft] | AOA ° | Nz [g] |
|---|---|---|---|---|
| C1S225 | | | -3.6 | -2.25 |
| C1S450 | | 5000 | 7.3 | 4.5 |
| C1S825 | 0.7 | | 15.9 | 8.25 |
| C2S225 | | | -5.4 | -2.25 |
| C2S450 | | 15000 | 10.5 | 4.5 |
| C2S825 | | | 26.6 | 8.25 |
| C3S225 | | | -1.8 | -2.25 |
| C3S450 | | 5000 | 4.1 | 4.5 |
| C3S825 | 0.9 | | 7.9 | 8.25 |
| C4S225 | | | -2.5 | -2.25 |
| C4S450 | | 15000 | 5.4 | 4.5 |
| C4S825 | | | 12.8 | 8.25 |

Table 3: ASIP load cases

The extreme load factors (-2.5 and 8.25) are present in this list as well as the points in the sky (Mach 0.7, 0.9, alt. 5'000 15'000) which are relevant for the Swiss fatigue spectrum.
The load case C1S825 was applied during the full scale fatigue test, and was computed using the original and recently with the new mesh. For this case the centre of pressures (CP) of the major aircraft components was calculated using the original mesh and the new mesh. These CP's were compared with the data from the ASIP study for this load case. Figure 5 shows that the CP's match overall very well, except for small differences on the centre fuselage, on the aft fuselage and on the TEF. From these results it is concluded that the CFD calculation is able to provide overall the correct load distributions for the major components.

| | SWISS ASIP | CFD original mesh | CFD new mesh |
|---|---|---|---|
| FWD FUSE + LEX | 34669 | 46741 | 46870 |
| CTR FUSE | 31772 | 49148 | 49409 |
| AFT FUSE | 6399 | 5184 | 4532 |
| FUSE. GLOBAL | 72840 | 101073 | 100811 |
| INNER WING | 40729 | 41616 | 41051 |
| OUTER WING | 15196 | 11799 | 12164 |
| ILEF | 24668 | 16252 | 16003 |
| OLEF | 10619 | 3828 | 3894 |
| TEF + SHROUD | 11076 | 14323 | 14665 |
| AILERON + SHROUD | 2905 | 4895 | 5236 |
| WING TOT | 105193 | 92713 | 93012 |
| HZT. TAIL RH | -1764 | 8752 | 7356 |
| AIRCRAFT TOT | 281322 | 304457 | 301464 |
| AIRCRAFT W/O VT & HT | 283226 | 286500 | 286835 |

Table 4: $F_Z$ in lbs for the load case C1S825 (ASIP).

Table 4 provides the $F_Z$ forces following the ASIP study together with the calculated results using the original and new mesh. The comparison between ASIP and CFD results gives the following results:

| | |
|---|---|
| HT | lift down instead of lift up |
| OLEF | about 3 times more lift |
| ILEF | 54 % more |
| AILERON+SHROUD | 44 % less |
| CTR FUSELAGE | 35 % less |
| OUTER WING | 25 % more |
| FWD FUSELAGE | 26 % less |
| AFT FUSELAGE | 41 % more |
| TEF+SHROUD | 24 % less |

It is interesting to see that for the total aircraft $F_Z$ the difference is 8%, and without HT the difference is only 1%. It should be mentioned that the CFD calculations matched the F4 US Navy flight data much better than the Swiss ASIP loads. The Swiss ASIP loads were determined from the F4 US Navy flight data by transformation to the correct point in sky and configuration. It is interesting to observe that the computed HT $F_Z$ for the ASIP loads do not show the correct trend, while the HT $F_Z$ for the F4 US Navy flight data base was predicted quite well. This leads to the conclusion that the simple engineering loads approach used during the Swiss ASIP study seems to have some draw backs. The flight data was inter- or extrapolated based on a simple AOA dynamic pressure curve which may not take into account the local flow field on all the control surfaces. These results demonstrate the powerful CFD technology for today's loads calculation.

### 4.3 Influence of the LEX Fence

With the new mesh it was possible to analyse the impact of the LEX fence on the structure of the flow field (see Fig. 6). The LEX fence has been placed on the LEX in order to fix the vortex separation and to reduce the aerodynamic excitation on the vertical tail. This excitation called buffeting caused fatigue problems of the vertical tail structure.

The differences in flow due to the LEX fence could be observed by steady state calculations. Figure 10 shows this influence on the $F_Z$ for three components: the fuselage, the wing components, and the vertical tail. As expected the influence on the vertical tail is enormous. The figures 7 and 9 illustrate perfectly this behaviour. The LEX fence has an influence upstream on the fuselage and the LEX itself. It affects sensibly the centre, the aft fuselage, the wing root as well as the inboard leading edge flap. The LEX fence changes in a relevant way the flow field around the vertical tail according to its original task (reduction of the buffeting impact).

These results prove that today's CFD technology is able to catch the effect of a small fin placed on the airframe, qualitatively by comparing the flow field with and without fin, quantitatively by calculating the corresponding component forces.

### 4.4 Force Distribution on the Wing

During the development of the full scale fatigue test facility the load distribution on the wing of the F/A-18 was a permanent issue. The values delivered by the OEM were for instance very high on the leading edge region. In order to establish a valid comparison the wing has been subdivided in 56 non-overlapping panels covering the leading edge flap, the wing torsion box, the trailing edge flap, the aileron and the tip launcher plus missile. This diagram is called Manhattan plot.

The distribution in the Manhattan plot of the CFD calculation looks smoother than the ASIP distribution and seems for this reason to be more corresponding to the physical reality. The huge outboard leading edge forces and the abrupt decrease of the trailing edge forces in the ASIP distribution have probably been necessary to adjust the hinge moments and the wing section forces to the F4 flight data base, to create the required bending and torsion moment at the wing fold and wing root, and finally to balance the overall aircraft.

All structural analysis of the wing during the ASIP study was based on this pronounced leading edge loading. The new CFD loads data will require a re-analysis of the assessment of the structural integrity.

### 4.5 CFD Calculation on the deformed Wing

The load case C1S825 corresponds to an 8.25 g steady state manoeuvre. At this condition the wing deforms due to the high loads, and one can expect that this change in wing shape will influence the flow over the wing. To investigate this effect an iterative CFD calculation on a flexible F/A-18 wing (with control surfaces) was made. Four iteration steps were needed to reach a converged wing position. During this simulation the fuselage, horizontal stabilizer, vertical tail and rudder were considered as rigid.

The simulation started with the rigid airframe on which the aerodynamic forces are calculated using CFD. These forces are transmitted to the NASTRAN model, which calculates in return the wing deformation. This deformation corresponds to the first iteration, and is applied on the CFD mesh to reshape it around the wing. This procedure was repeated until a converged wing position was obtained.

The deformed wing is shown in figure 11. Note that the missile remains almost parallel to itself; hence we are facing a pure bending deformation mode. It can also be seen that the difference in the spatial angle between TEF and aileron was reduced by the deformation of the wing.

The first iteration produced a large deflection. The second and subsequent iterations bring only small corrections, and the third and fourth iterations are almost identical.
The wing bending moment was calculated for all four iterations, and for this quantity the fast convergence was observed as well. A large effect of the wing deformation was observed, since this quantity was reduced with 16% compared to the non-deformed wing.

### 4.6 Sensitivity Analysis of the CFD Calculations

All calculations discussed in the previous sections were made using the Spalart-Allmaras turbulence model. This model was developed for aerospace applications, and in general provides satisfactory results. For highly separated flows, the k-ω model, and in particular the Menter Shear Stress (MSS) variant has received recently much attention.
Due to the high angle of attack for the 8.25 g steady state manoeuvre, large regions of unsteady and separated flow are present. For this reason the $C_L$ convergence histories showed oscillations. One of these 8.25 g manoeuvre was calculated using the k-ω MSS model, and Table 5 summarizes the aerodynamic coefficients and the $N_Z$ for the 2 computations. The differences are small, with the computation using the k-ω model yielding a slightly higher $N_Z$ which is closer to the expected value.

| Case | $C_L$ | $C_D$ | $C_M$ | com Nz | exp Nz |
|---|---|---|---|---|---|
| Spalart | 1.287 | 0.561 | 0.154 | 8.06 | 8.25 |
| k-ω | 1.294 | 0.563 | 0.170 | 8.11 | 8.25 |

Table 5: aerodynamic coefficients for Spalart and k-ω turbulence model

Small differences in the pressure contours ($p - p\infty$) can be observed on the upper side of the horizontal stabilizer, on the vertical fin, and on the fuselage downstream of the wing attachment. On the lower side differences can only be observed on the horizontal stabilizer. In the plane at x = 16 m (the reference position of the vertical tail) large separated flow regions could be observed, and differences in computed results were visible. However, it should be remarked that the flow is unsteady, and differences may not only come from the turbulence model, but also from the unsteadiness of the flow.

Besides the influence of the turbulence model, the influence of the Mach number, of the angle of attack (AOA), and the deflection of all control surfaces on the F/A-18 was analyzed. The change of the angle of attack (AOA) was very remarkable because it affects the lift of the airplane. A difference of only 1° in angle of attack may change the $C_L$ value by 20%. The same chance of the deflection angle of the control surfaces showed only a small influence on the aerodynamic coefficient $C_L$, $C_D$, and $C_M$.
The influence of a change of the Mach number in the order of 0.02 showed for the aerodynamic coefficients a very small impact of 2% which is within the order of the accuracy of the CFD computation.

## 5. Conclusion

### 5.1 Achievements

The NSMB solver with the multi block structure is a very flexible and robust tool. It allowed us to generate a huge amount data in relation with the aerodynamic behaviour of the F/A-18. The main tasks fulfilled until now are the following:

- determination of global and component loads on the aircraft at high angle of attack and at transonic flight conditions
- flow field visualization for a better understanding of the aerodynamic behaviour
- analysis of the effect of small fins on lifting surfaces like the vertical tail
- evaluation of the influence of wing deformation on the aerodynamic forces

Until now these calculations were made for symmetrical load cases so that only a half aircraft had to be modelled. A-symmetrical load cases require a doubling of the mesh, but since the critical load cases with high angle of attack are all symmetrical, this his a lower priority.

### 5.2 Outlook

The next step in the CFD project is to calculate the unsteady flow field at high angle of attack, and to evaluate the unsteady forces of the LEX vortex acting on the vertical tail. The LEX fence will be taken into account in this study in order to analyse its effect.

The objective of these calculations is to set up a model of unsteady forces on the vertical tail applicable for the different manoeuvres at various angles of attack. This model will afterwards allow us to determine the stresses, for instance at the vertical tail root, which is a structural critical part, and to develop fatigue spectra representing the service flight of the Swiss F/A-18.

Another ambitious project is to use the CFD for aero-elastic calculations. This new step can be considered as an extension of the CFD calculation on a deformed wing. In this case the deformation is not static but dynamic in the same frequency range like the unsteady flow field.

This simulation is clearly more complex, as it requires the development of new algorithms and it is very CPU time consuming. The interest of aero-elasticity in this case is to investigate the flight conditions, in which the unsteady flow interacts with the dynamic structural deformations in a way to produce instability.

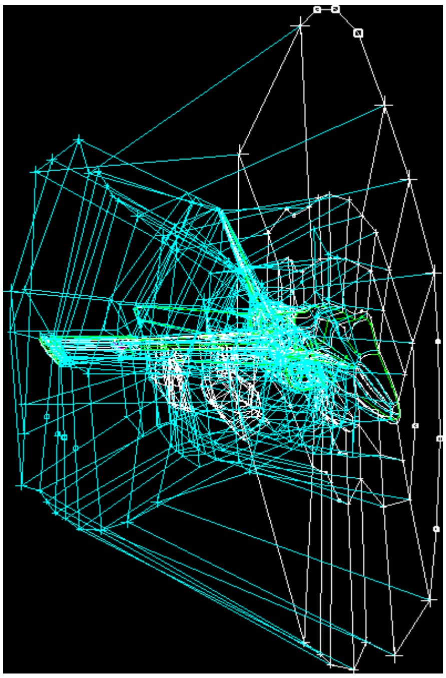

Fig. 1: blocks around the F/A-18

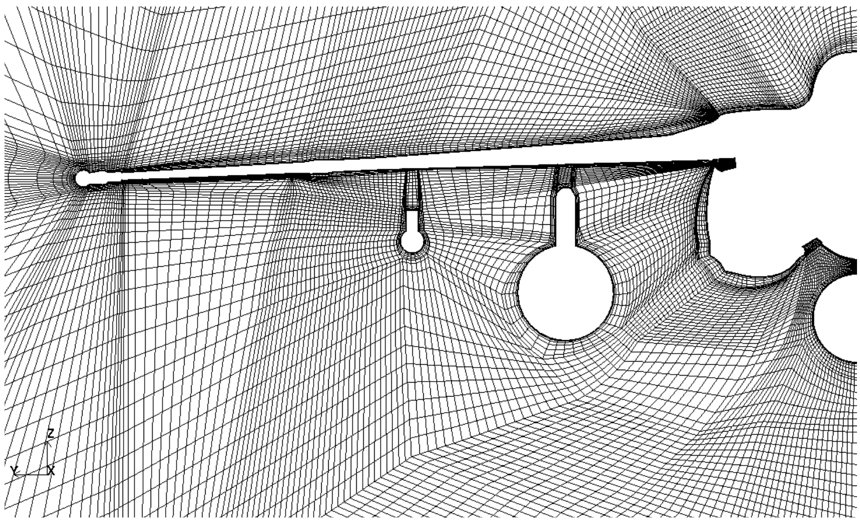

Fig. 2: cut in the mesh of the F/A-18

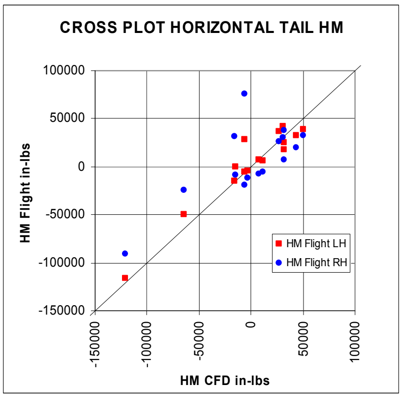


Fig. 3: ILEF hinge moment crossplot

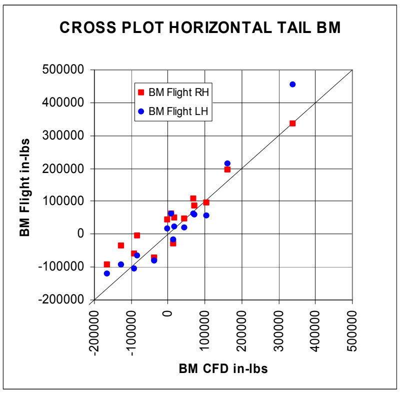


Fig. 4: OLEF hinge moment crossplot

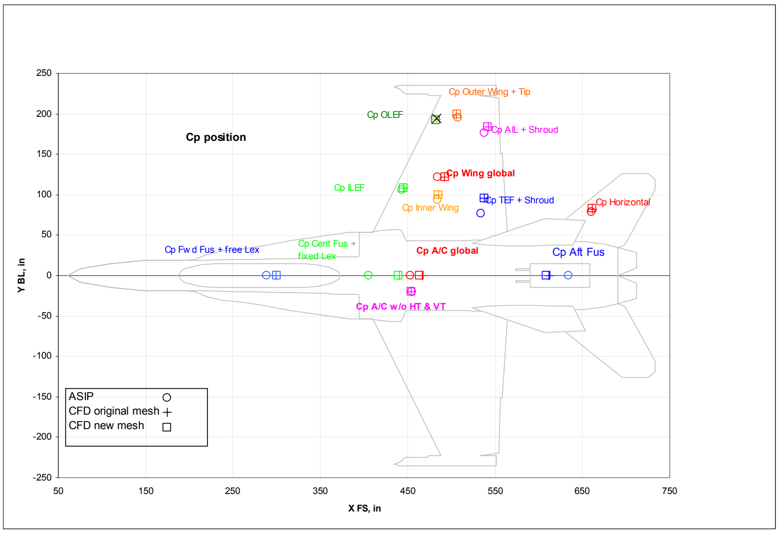


Fig. 5: centre of pressure comparison for ASIP & CFD


Fig. 6: LEX fence

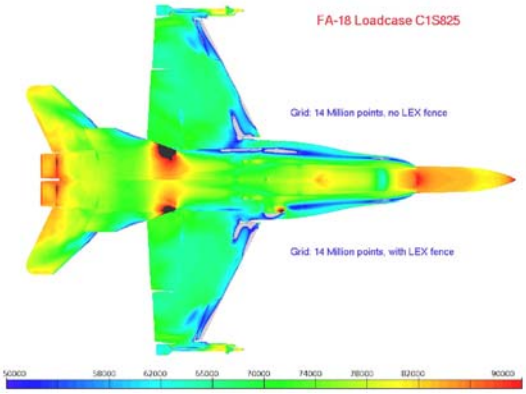


Fig. 7: pressure distribution (upper side) with & W/O LEX fence

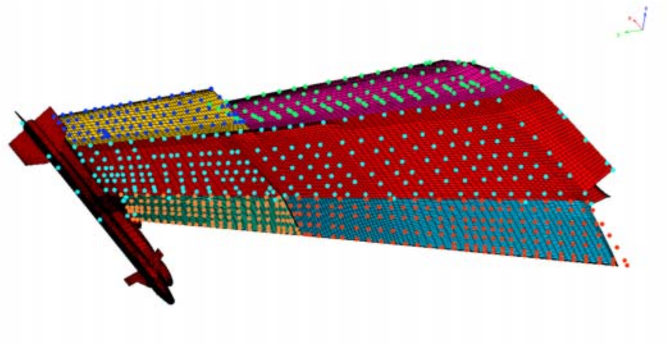

Fig. 8: CFD grid and structure grid (FEM) superimposed

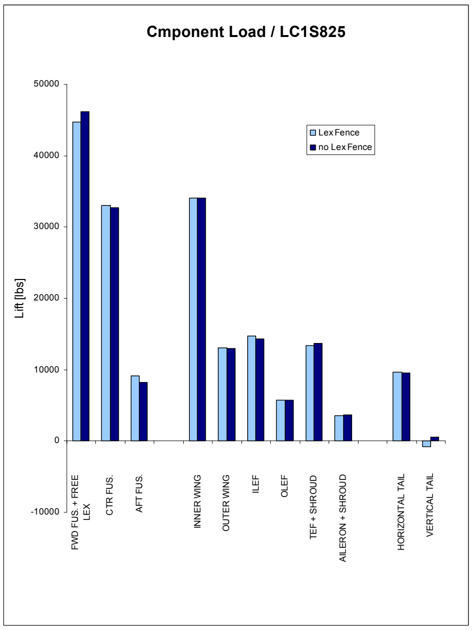


Fig. 9: component forces with & W/O LEX fence

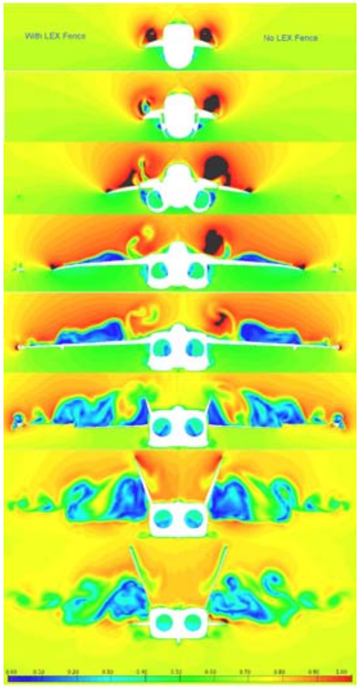


Fig. 10: flow with & W/O LEX fence

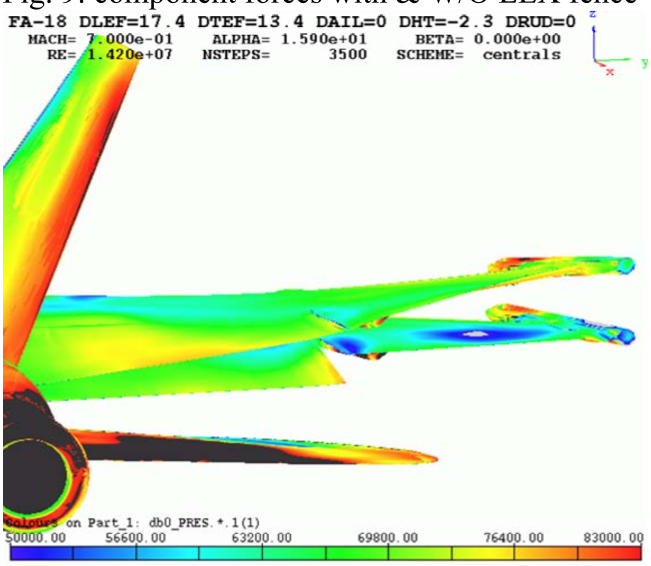


Fig. 11: CFD result of undeformed and deformed wing using fluid structure coupling